Loss of Microtubule Associated Protein 2 Immunoreactivity Linked to Dendritic Spine Loss in Schizophrenia

Supplemental Information

Supplemental Methods

Human Subjects

Brain tissue was obtained during autopsies conducted at the Allegheny County Office of the Medical Examiner, after receiving consent from next-of-kin using a mechanism approved by the University of Pittsburgh Institutional Review Board and Committee for Oversight of Research Involving the Dead. An independent committee of experienced clinicians made consensus DSM-IV (Diagnostic and Statistical Manual of Mental Disorders, 4th ed.) diagnoses for each subject, using information obtained from clinical records and structured interviews with surviving relatives as previously described (1, 2).

Human Tissue Processing

Brains from individuals in cohorts 1 and 2 were bisected and the left hemisphere was cut into 1-2 cm thick coronal blocks, which were then immersed in 4% paraformaldehyde in phosphate buffer for 48 hours, equilibrated in a series of graded sucrose solutions, and stored at -30˚C in an antifreeze solution.

The left superior temporal gyrus (STG) of each subject was dissected from fixed coronal blocks; reassembled in their *in vivo* orientation, and cut into 3 mm thick slabs as previously described (3). Every other slab was selected, sectioned exhaustively, and adjacent sections stained for parvalbumin, acetylcholinesterase, and Nissl substance for determination of the boundaries of the primary auditory cortex (3). For each human and monkey subject, the borders of layers 2/3 and 3/4 were identified on the mapping sections to determine the total layer 3 area

for each subject. A contour outline of the deepest one third of layer 3 was drawn in Stereo Investigator (Figure 1, MicroBrightField Inc., Colchester, Vermont). These contours were then aligned to the tissue sections used in the current study using pial surface fiduciaries.

For cohort 1, the primary auditory cortex was dissected from the unused slabs, and further subdivided into 3 mm wide blocks which were sectioned at 50 µm in an orientation perpendicular to the pial surface, and stored in antifreeze solution at -30˚C until selected for use in this study as described previously (4-6). For cohort 2, 60 µm sections adjacent to the mapping sections were sampled systematic uniform random for assay (Figure 1).

Antipsychotic-exposed Monkey Cohort

Over a period of 9-12 months, macaques were intramuscularly administered the antipsychotic haloperidol decanoate every four weeks at a dose [mean (standard deviation)] of 16 (2.1) mg/kg which maintained trough serum levels at 4.3 (1.1) ng/ml. Similar concentrations have been associated with a therapeutic response in humans (7), and resulted in extrapyramidal symptoms, which were effectively controlled in all treated animals with benztropine mesylate.

At the end of haloperidol exposure, all animals were euthanized by pentobarbital overdose; brains were removed and immersed in 4% paraformaldehyde following a 45 minute postmortem interval (PMI). Primary auditory cortex was identified in sections from the STG using previously described cytoarchitectonic and immunohistochemical features (8). All protocols were approved by the University of Pittsburgh's Institutional Animal Care and Use Committee.

Immunohistochemistry

A single tissue section per subject was included in each run along with its matched pair for a total of 3-4 sections per subject from cohort 1 and 3 sections per subject from cohort 2. In order to visualize dendritic spines, we used two markers in combination: a polyclonal antibody

directed against spinophilin and raised in rabbit (Millipore AB5669, Billerica, MA) at a dilution of 1:1500. The second was the f-actin binding mushroom toxin phalloidin (Invitrogen A12380, Carlsbad, CA) conjugated to Alexa Fluor® 568. Spinophilin is highly enriched in spine heads (9,10). Phalloidin binds f-actin which is also highly enriched in dendritic spines (11). These two labels show clear co-localization in structures resembling dendritic spines in human postmortem brain tissue (Figure 2). MAP2 was detected through the use of mouse monoclonal IgG antibody SMI-52 (Covance SMI-52R, Princeton, NJ) at a dilution of 1:500. SMI-52 has been shown to react with mammalian MAP2 both in culture and in fixed sections, robustly labeling the soma and dendritic arbor of neurons in human tissue (12). In immunoblot experiments, SMI-52 recognizes all isoforms of MAP2 (MAP2A, MAP2B, MAP2C) (13). Free-floating sections were pre-treated with 1% $NaBH_4$ to reduce auto-fluorescence and 0.3% Triton X in order to permeabilize the sections before being incubated for two hours at room temperature in blocking buffer comprised of 20% normal human serum, 20% normal goat serum, 1% bovine serum albumin, 0.1% lysine, 0.1% glycine, and phosphate buffered saline (PBS). Following blocking, tissue was immediately placed in primary antibody buffer (5% normal human serum, 5% normal goat serum, 1% bovine serum albumin, 0.1% lysine, 0.1% glycine, PBS, and antibodies) overnight at 4˚C. Sections were rinsed in PBS then incubated in the same buffer, containing biotinylated goat anti-mouse (1:250; Invitrogen BA-9200), Alexa Fluor® 488 goat anti-rabbit (1:500; Invitrogen A11034), and Phalloidin- Alexa Fluor® 568 (3:200) at 4˚C for 24 hours. Tissue was again rinsed then incubated overnight in a 1:500 dilution of streptavidin Alexa Fluor® 647 (Invitrogen, S32357) at 4˚C. The tissue sections were subsequently mounted on gel-coated slides, rehydrated to ameliorate the effects of z-axis tissue shrinkage, and coverslipped using Vectashield hard-set H-1400 mounting medium (Vector Laboratories, Burlingame, CA). Sections from the antipsychotic- and control monkeys were processed together within immunohistochemistry runs using identical procedures.

Image Collection

All images were taken using a 1.42 numerical aperture 60X oil supercorrected objective mounted on an Olympus BX51Wl upright microscope (Olympus, Center Valley, PA) equipped with an Olympus DSU spinning disk, Hamamatsu Orca R2 camera (Hamamatsu, Bridgewater, NJ), MBF CX9000 front mounted digital camera (MicroBrightField Inc., Natick, MA), BioPrecision2 XYZ motorized stage with linear XYZ encoders (Ludl Electronic Products Ltd., Hawthorne, NY), excitation and emission filter wheels (Ludl Electronic Products Ltd., Hawthorne, NY), Sedat Quad 89000 filter set (Chroma Technology Corp., Bellows Falls, VT), and a Lumen 220 metal halide lamp (Prior Scientific, Rockland, MA). The process of image collection was accomplished using Slidebook software version 5.027 (Intelligent Imaging Innovations, Denver, CO) and Stereo Investigator version 8 (MicroBrightField Inc., Natick, MA).

Calculation of Spine Density and Number

Phalloidin mask objects overlapping spinophilin mask objects were counted automatically by determining whether the centroid of each automatically detected object was inside the disector. This corresponds to the so-called “associated point rule” (14), which is an unbiased alternative to the unbiased counting frame (15). Guard zones of 10 pixels were applied around all edges in the X and Y dimensions of each stack, and a guard zone of 4 Z planes was provided starting at the top of the tissue below the coverglass. The resulting disectors were 492 x 492 pixels in X and Y dimensions, and 24 Z planes (cohort 1) or 4 Z planes (cohort 2). These Z ranges were selected based on evidence from calibration plots that puncta counts and intensities were uniform across these Z axis depths. It should be noted that the relatively low disector height (1.0 µm in Cohort 2) could be implemented robustly because we used confocal microscopy allowing for a high number of thin focal planes, because of our use of deconvolution with full thickness reconstructions and determination of centroids; and because we performed a careful analysis of the distribution of the puncta along the Z axis. We determined the position of the disector and

corresponding guard zones *post hoc* ensuring that puncta were only sampled in the zone with uniform bouton counts. Such sampling was also possible due to the high number of automatically detected puncta per subject. Thus, while a disector height of only 1.0 µm should be avoided in a standard brightfield microscopy study with manual counts, we were able to robustly implement such a disector in the current study.

Statistical Models

Human Tissue Study

For each subject in the human tissue study, the intensity of MAP2-IR was first log transformed to more normally distribute MAP2-IR data. To assess the diagnostic effect in log MAP2-IR, spine density, spine number and deep layer 3 volume, two analysis of covariance models were used. Because we paired subjects within each cohort on age, sex, and postmortem interval, the primary model included diagnosis, cohort (which in this case includes effects of assay run and imaging run because the cohorts were studied sequentially), pair nested within cohort as blocking factors and tissue storage time (which is not a pairing variable, but may affect assay fidelity) as a covariate. To then assess the robustness of results, a secondary model was used with diagnosis, cohort, and tissue storage time as covariates, and in place of subject pairings, we instead entered as covariates the pairing variables: age, sex, and postmortem interval.

In order to examine the confound effect of each of the following factors: sex (F/M), manner of death (suicide), diagnostic variation [schizoaffective disorder (Y/N)], age of onset, duration of disease, antipsychotic use (Y/N), anticonvulsant use (Y/N), benzodiazepine use (Y/N), non-diagnosis related drug treatment (Y/N), and substance abuse/dependence at time of death [alcohol (Y/N), tobacco (Y/N), cannabis history (Y/N), non-specified (Y/N)], the pairwise percent difference in each of the four variables was analyzed. If the confound variable was dichotomous, a two sample *t* test was used. If the confound variable was continuous, a simple

linear regression analysis was used. The percent difference in log MAP2-IR within a pair is calculated as:

$$\frac{(\log(\text{MAP2 intensity}) \text{ in Control} - \log(\text{MAP2 intensity}))}{\log(\text{MAP2 intensity}) \text{ in Control}} \; X \; 100\%.$$

The pairwise percent differences for other variables were calculated similarly.

The relationship between log MAP2-IR and spine density was determined by two methods: Pearson's correlation coefficient and alternatively optimized Kendall's tau. In order to examine the relationship between log MAP2-IR and spine density, both variables were dichotomized by choosing cutoff points. A 2 by 2 contingency table was calculated for each chosen set of cutoff points. Kendall's tau was used as the measure of association of the contingency table. An optimizing search was used to find the cutoff points for each of log(MAP2-IR) and spine density so that Kendall's tau was maximized. The asymptotic *p*-value was obtained for the Kendall's tau to test if it is different from 0.

Diagnostic effect in spine density and spine numbers were examined within the MAP2 Low and MAP2 Normal subgroups using the same primary and secondary models used on the entire 20 pairs of subjects.

The analyses for diagnosis effect and confound effect were implemented in SAS PROC GLM with alpha 0.05; Kendall's tau was obtained in SAS PROC FREQ, and the Pearson correlation coefficient was obtained in SAS PROC CORR.

Monkey Tissue Study

For each observation in the monkey tissue study, log MAP2-IR was taken before analysis so that MAP2 intensity was more normally distributed. Haloperidol treatment effect was examined with two mixed effect models: a primary model with treatment, assay and pair as fixed effect and monkey as a normal random effect to account for the repeated measures within one monkey; the secondary model was the same as the primary model except that pair was not

included in the model. The analyses for the monkey tissue study were implemented in SAS PROC MIXED with alpha = 0.05.

Supplemental Results

Primary Auditory Cortex Deep Layer 3 Neuron Number in Cohort 1 Subjects

We previously reported that pyramidal neuron number did not differ between control subjects and schizophrenia subjects in individuals from cohort 1 (4). Mean layer 3 pyramidal neuron number for control subjects was 3.38×10^6 and 4.11×10^6 for schizophrenia subjects, a non-significant difference ($F_{1,10} = 1.25$; $p = 0.29$) The relationship between MAP2-IR and pyramidal neuron number is show in Figure S1). This finding confirms that MAP2-IR loss is not a result of pyramidal neuron loss.

MAP2 Peptide Amount in Primary Auditory Cortex Deep Layer 3

MAP2-IR loss could reflect a loss of protein, or a reduction in the ability to bind to its epitope. To determine if MAP2-IR loss is driven by a loss of protein, total protein was extracted from gray matter homogenates obtained from Heschl's gyrus containing the primary auditory cortex as previously described (16). Five MAP2 peptides representing sequences along the length of MAP2 protein (Figure S2, Top) were quantified using liquid chromatography-mass spectrometry with selected reaction monitoring and quantification via a stable isotope labeled mouse brain standard as previously described (17). MAP2 peptides were quantified in 5 pairs of subjects from the present study in whom the schizophrenia subject exhibited MAP2-IR values below the lowest control value observed in the entire cohort, deemed MAP2-IR Low. We found no significant differences in MAP2 peptide levels, despite substantial reductions in MAP2-IR in these same subject pairs (Figure S2, Bottom).

MAP2-IR by Postmortem Interval

We found no significant effect of PMI in log MAP2-IR based on our secondary model in which the term pair is replaced by age, PMI, and sex ($F_{(1,33)} = 0.06$, $p = 0.81$; Figure S3).

Table S1. Association of clinical variables with spine density, spine number, and MAP2-IR, with the Differences within Pairs (C-S).

Dependent	Measure	Number		Estimate	Std. Error	t-Value	*p*
		Control	Sz				
MAP2-IR	Sex (M/F)	13/7	13/7	0.2394	0.2420	0.9894	0.3356
	Suicide (Y/N)	0/20	4/16	-0.4052	0.2805	-1.4444	0.1658
	Schizoaffective (Y/N)	N/A	6/14	-0.3154	0.2477	-1.2731	0.2192
	Antidepressant (Y/N)	0/0	8/12	0.1419	0.2396	0.5920	0.5612
	Antipsychotic (Y/N)	0/0	17/3	-0.0531	0.3317	-0.1599	0.8747
	Anticonvulsant (Y/N)	0/0	6/14	0.2191	0.2535	0.8645	0.3987
	Benzodiazepine (Y/N)	0/0	4/16	-0.4314	0.2783	-1.5498	0.1386
	Alcohol dependence/abuse ATOD (Y/N)	0/0	4/16	0.0991	0.2954	0.3354	0.7412
	Cannabis history (Y/N/U)	2/17/1	7/13/0	0.1775	0.2450	0.7248	0.4779
	Tobacco ATOD (Y/N/U)	7/11/2	14/5/1	-0.1652	0.2794	-0.5913	0.5621
	Other substance abuse ATOD (Y/N)	0/0	2/18	-0.2747	0.3898	-0.7048	0.4900
	Age of onset (Y/N)	N/A		-0.0143	0.0143	-0.9977	0.3317
	Duration of disease (Y/N)	N/A		0.0021	0.0088	0.2327	0.8186
Spine Density	Sex (M/F)	13/7	13/7	0.0058	0.0053	1.1003	0.2857
	Suicide (Y/N)	0/20	4/16	-0.0045	0.0064	-0.7003	0.4927
	Schizoaffective (Y/N)	N/A	6/14	-0.0055	0.0055	-0.9903	0.3351
	Antidepressant (Y/N)	0/0	8/12	-0.0024	0.0053	-0.4450	0.6617
	Antipsychotic (Y/N)	0/0	17/3	-0.0116	0.0068	-1.7133	0.1038
	Anticonvulsant (Y/N)	0/0	6/14	0.0014	0.0057	0.2488	0.8063
	Benzodiazepine (Y/N)	0/0	4/16	0.0000	0.0065	-0.0044	0.9965
	Alcohol dependence/abuse ATOD (Y/N)	0/0	4/16	-0.0037	0.0065	-0.5654	0.5788
	Cannabis history (Y/N/U)	2/17/1	7/13/0	0.0052	0.0053	0.9684	0.3457
	Tobacco ATOD (Y/N/U)	7/11/2	14/5/1	-0.0055	0.0059	-0.9298	0.3655

Dependent	Measure	Number		Estimate	Std. Error	t-Value	*p*
		Control	Sz				
Spine Density	Other substance abuse ATOD (Y/N)	0/0	2/18	-0.0003	0.0087	-0.0398	0.9476
	Age of onset	N/A		-0.0026	0.0089	-0.2869	0.7774
	Duration of disease	N/A		-0.0050	0.0052	-0.9554	0.3520
Spine Number	Sex (M/F)	13/7	13/7	0.2426	0.2635	0.9207	0.3694
	Suicide (Y/N)	0/20	4/16	-0.3140	0.3129	-1.0036	0.3289
	Schizoaffective (Y/N)	N/A	6/14	-0.0432	0.2804	-0.1540	0.8793
	Antidepressant (Y/N)	0/0	8/12	-0.4473	0.2404	-1.8607	0.0792
	Antipsychotic (Y/N)	0/0	17/3/0	-0.3873	0.3484	-1.1116	0.2809
	Anticonvulsant (Y/N)	0/0	6/14	0.3944	0.2648	1.4895	0.1537
	Benzodiazepine (Y/N)	0/0	4/16	-0.2010	0.3180	-0.6320	0.5353
	Alcohol dependence/abuse ATOD (Y/N)	0/0	4/16	0.3292	0.3120	1.0552	0.3053
	Cannabis history (Y/N/U)	2/17/1	7/13	0.3058	0.2598	1.1771	0.2545
	Tobacco ATOD (Y/N/U)	7/11/2	14/5/1	0.0063	0.2826	0.0223	0.9825
	Other substance abuse ATOD (Y/N)	0/0	2/18	-0.0822	0.4282	-0.1919	0.8499
	Age of onset	N/A		0.0027	0.0103	0.2671	0.7924
	Duration of disease	N/A		0.0025	0.0061	0.4039	0.6911

ATOD, at time of death; F. female; M, male; N, no; Sz, schizophrenia; U, unknown; Y, yes.

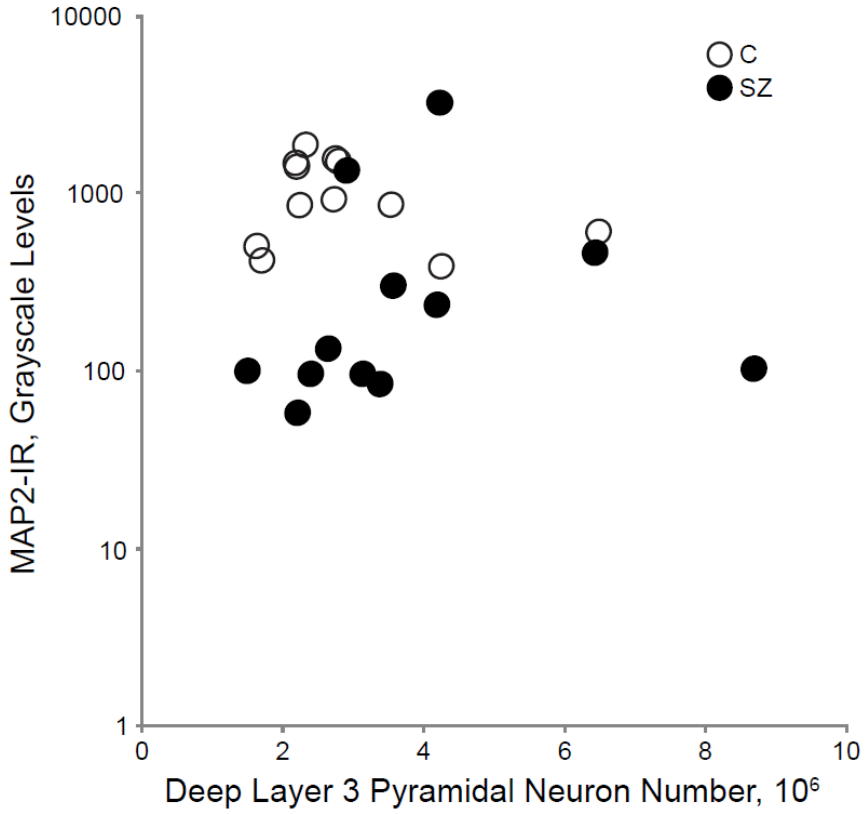

Figure S1. MAP2-IR reductions in cohort 1 do not reflect loss of pyramidal neuron number in deep layer 3 of primary auditory cortex. MAP2-IR plotted as a function of deep layer pyramidal neuron number in primary auditory cortex in control subjects (open circles) and schizophrenia subjects (filled circles) from cohort 1. For all subjects, r^2 = 0.013; the corresponding values for control, r^2 = 0.0828 and schizophrenia subjects, r^2 = 0.0047. None of the correlations were significant.

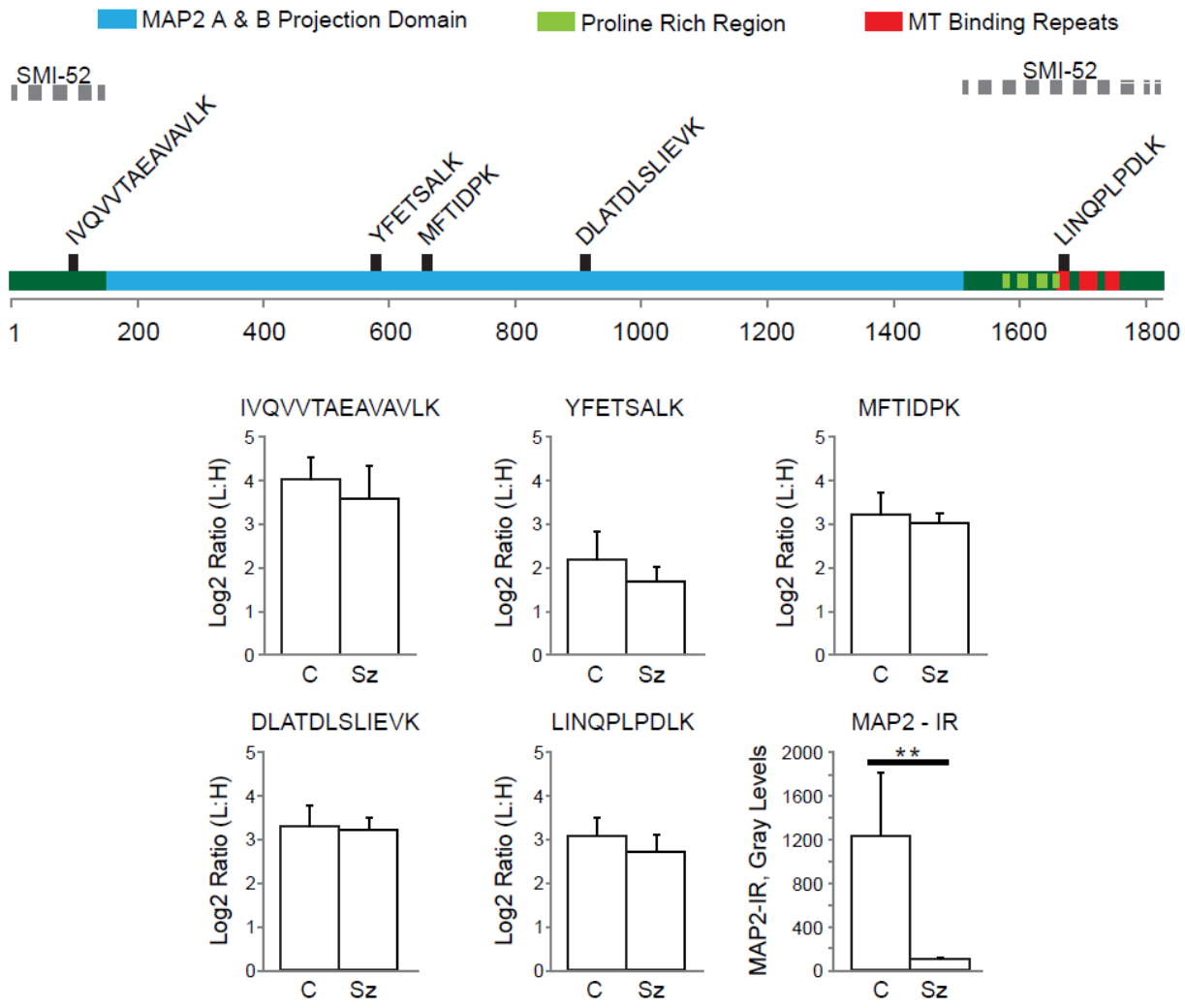

Figure S2. MAP2 peptide levels are unchanged in MAP2-IR Low Sz subjects. (**Top**) Schematic of MAP2 protein isoforms. Dark green shows amino acids included in isoform MAP2C, whereas MAP2A and MAP2B also include the projection domain shown in blue. The locations of other functional domains along the length of MAP2 (numbering indicates amino acids) are as indicated. Dashed gray lines indicate the potential regions within MAP2 to which antibody used in this study (SMI-52, Covance) binds. The peptide sequences used for subsequent quantification are shown in their respective locations within the MAP2 protein. (**Bottom**) Mean ratios of MAP2 peptides in five MAP2-IR Low pairs (control, C; schizophrenia, Sz). Mean MAP2-IR for the same 5 pairs is shown in last panel. ** $p < 0.01$. Error bars are standard deviations.

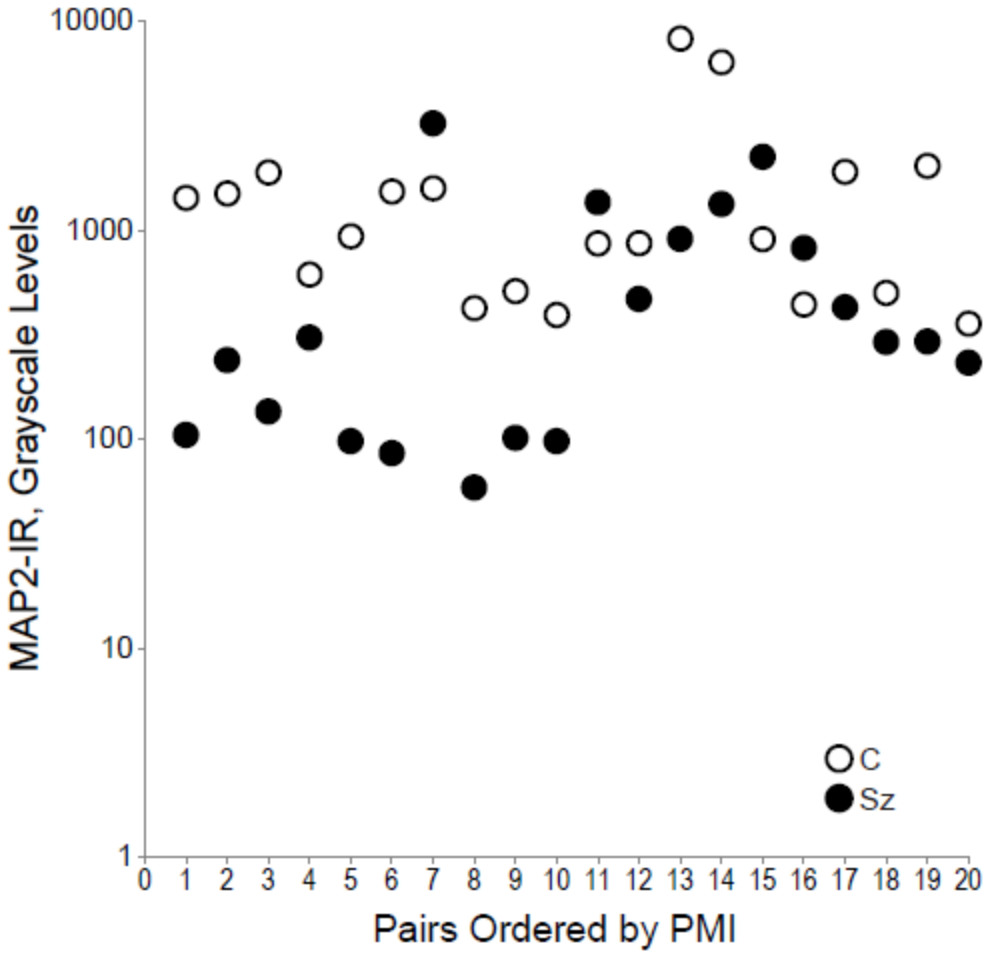

Figure S3. MAP2-IR is unaffected by PMI. We found no significant effect of PMI on MAP2-IR. MAP2-IR is shown for each pair in order (from left to right) of ascending PMI of the Sz subjects. Control subjects open circles; schizophrenia subjects, filled circles.

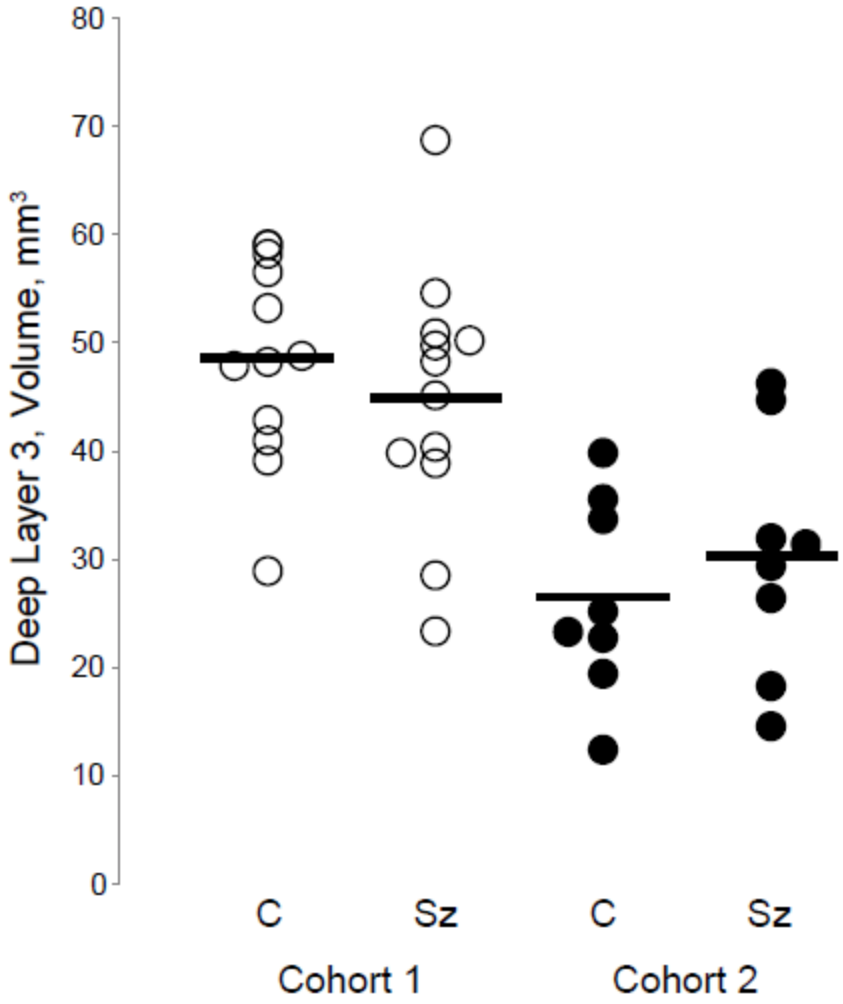

Figure S4. MAP2-IR is unaffected by BA41 deep layer 3 volume. We found no significant difference in BA41 deep layer 3 volume between control subjects (open circles) and schizophrenia subjects (filled circles). For cohort 1, primary auditory cortex volumes were previously determined (4). For cohort 2, primary auditory cortex was systematic uniform random sampled, yielding 3-9 sections per subject, and volumes were determined using the Cavalieri method with a mean coefficient of error of 0.095. Deep layer 3 volumes for cohort 1 and 2 were then determined as previously described (5).

Supplementary References

1. Glantz LA, Lewis DA (2000): Decreased dendritic spine density on prefrontal cortical pyramidal neurons in schizophrenia. *Arch Gen Psychiatry* 57:65-73.

2. Sweet RA, Henteleff RA, Zhang W, Sampson AR, Lewis DA (2009): Reduced dendritic spine density in auditory cortex of subjects with schizophrenia. *Neuropsychopharmacology* 34:374-89.

3. Sweet RA, Dorph-Petersen KA, Lewis DA (2005): Mapping auditory core, lateral belt, and parabelt cortices in the human superior temporal gyrus. *J Comp Neurol* 491:270-89.

4. Dorph-Petersen KA, Delevich KM, Marcsisin MJ, Zhang W, Sampson AR, Gundersen HJ*, et al.* (2009): Pyramidal neuron number in layer 3 of primary auditory cortex of subjects with schizophrenia. *Brain Res* 1285:42-57.

5. Moyer CE, Delevich KM, Fish KN, Asafu-Adjei JK, Sampson AR, Dorph-Petersen KA*, et al.* (2012): Reduced glutamate decarboxylase 65 protein within primary auditory cortex inhibitory boutons in schizophrenia. *Biol Psychiatry* 72:734-43.

6. Moyer CE, Delevich KM, Fish KN, Asafu-Adjei JK, Sampson AR, Dorph-Petersen KA*, et al.* (2013): Intracortical excitatory and thalamocortical boutons are intact in primary auditory cortex in schizophrenia. *Schizophr Res* 149:127-34.

7. Volavka J, Cooper T, Czobor P, Bitter I, Meisner M, Laska E*, et al.* (1992): Haloperidol blood levels and clinical effects. *Arch Gen Psychiatry* 49:354-61.

8. Sweet RA, Bergen SE, Sun Z, Sampson AR, Pierri JN, Lewis DA (2004): Pyramidal cell size reduction in schizophrenia: evidence for involvement of auditory feedforward circuits. *Biol Psychiatry* 55:1128-37.

9. Allen PB, Ouimet CC, Greengard P (1997): Spinophilin, a novel protein phosphatase 1 binding protein localized to dendritic spines. *Proc Natl Acad Sci U S A* 94:9956-61.

10. Muly EC, Smith Y, Allen P, Greengard P (2004): Subcellular distribution of spinophilin immunolabeling in primate prefrontal cortex: localization to and within dendritic spines. *J Comp Neurol* 469:185-97.

11. Capani F, Ellisman MH, Martone ME (2001): Filamentous actin is concentrated in specific subpopulations of neuronal and glial structures in rat central nervous system. *Brain Res* 923:1-11.

12. Anderson SA, Volk DW, Lewis DA (1996): Increased density of microtubule associated protein 2-immunoreactive neurons in the prefrontal white matter of schizophrenic subjects. *Schizophr Res* 19:111-9.

13. Kaufmann WE, Taylor CV, Lishaa NA (1997): Immunoblotting patterns of cytoskeletal dendritic protein expression in human neocortex. *Mol Chem Neuropathol* 31:235-44.

14. Baddeley AVJ, Eb. (2005): *Stereology for Statisticians*. Boca Raton, FL: Chapman & Hall/CRC.

15. Gundersen HJ (1977): Notes on the estimation of the numerical density of arbitrary profiles: the edge effect. *J Microscopy* 111:219-223.

16. Deo AJ, Cahill ME, Li S, Goldszer I, Henteleff R, Vanleeuwen JE*, et al.* (2012): Increased expression of Kalirin-9 in the auditory cortex of schizophrenia subjects: its role in dendritic pathology. *Neurobiol Dis* 45:796-803.

17. Macdonald ML, Ciccimaro E, Prakash A, Banerjee A, Seeholzer SH, Blair IA*, et al.* (2012): Biochemical fractionation and stable isotope dilution liquid chromatography-mass spectrometry for targeted and microdomain-specific protein quantification in human postmortem brain tissue. *Mol Cell Proteomics* 11:1670-81.